THE JOURNAL OF PHYSICAL CHEMISTRY C

Article

Cite This: J. Phys. Chem. C 2018, 122, 20918−20922

pubs.acs.org/JPCC

In Silico Optimization of Organic−Inorganic Hybrid Perovskites for Photocatalytic Hydrogen Evolution Reaction in Acidic Solution

Lu Wang,[†,‡] William A. Goddard, III,[*,‡,§] Tao Cheng,[‡,§] Hai Xiao,[‡,§] and Youyong Li[*,†]

[†]Institute of Functional Nano & Soft Materials (FUNSOM), Jiangsu Key Laboratory for Carbon-Based Functional Materials & Devices, Soochow University, Suzhou, Jiangsu 215123, China

[‡]Materials and Process Simulation Center (MSC) and [§]Joint Center for Artificial Photosynthesis (JCAP), California Institute of Technology, Pasadena, California 91125, United States

Supporting Information

ABSTRACT: We previously reported the atomistic reaction mechanism for the photocatalytic hydrogen evolution reaction (HER) on the $CH_3NH_3PbI_3$ organic−inorganic hybrid perovskites based on quantum mechanics calculations of the transition-state barriers, including several layers of explicit acidic solvent. Here, we extend these studies using in silico optimization to discover additional promising photocatalysts. We consider replacing (i) Pb with Sn, (ii) I with Br, and (iii) CH_3NH_3 cation with several organic cations, including $NH_2(CH)NH_2$ cation as the photocatalyst for HER. We compared the activation barriers and reaction energies for each case. In our previous studies, we found that both H atoms of the H_2 product are extracted from surface organic cations with protons from the solution migrating along Grotthuss water chains to replace the H of the organic cations. This two-step reaction mechanism involves formation of an intermediate lead hydride bond, with the lead atoms and the surface organic cations both playing essential roles. Among the perovskites investigated here, we predict that $NH_2(CH)NH_2PbI_3$ exhibits the best HER performance with a predicted 10-fold improvement in the reaction rate compared to $CH_3NH_3PbI_3$. We also suggest that the lead-free tin iodide perovskites might exhibit a rate comparable to that of lead iodide perovskites with the same organic cations. However, replacing iodine by bromine significantly increases the activation barrier. We find for these lead iodide perovskites, the increased proton affinity of the surface organic cations enhances the photocatalytic efficiency, with $NH_2(CH)NH_2$ the best case examined.

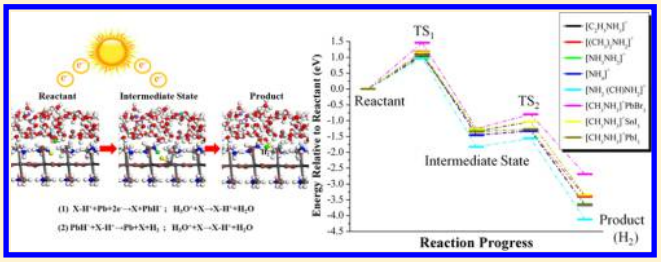

Photochemical generation of H_2 provides a potentially renewable process to address the energy and environmental issues without producing pollution. In early developments, TiO_2 photocatalysts loaded with small amounts of Pt or Rh nanoparticle were co-catalysts to generate H_2 by splitting water under the UV light.[1,2] Later, other metal oxides and metal sulfides, such as CdS and WO_3, were examined as heterogeneous photocatalysts.[3,4] Moreover, such two-dimensional nanomaterials as ZnSe, g-C_3N_4, and transition-metal chalcogenides have shown promise as efficient photocatalysts with a high specific surface area and long electron/hole diffusion distances.[5−7] More recently, organic−inorganic hybrid perovskites, such as $CH_3NH_3PbI_3$, have taken a dominant position in the photovoltaic field.[8,9] They can be fabricated by a simple, easy solution process and comprise earth-abundant elements, making them of low cost. Their outstanding properties, including optimal band gaps (1.5−2.0 eV), low exciton binding energy,[10] and long carrier lifetime,[11] provide promising routes to efficiently utilize sunlight for water splitting. The power conversion efficiency for the organic−inorganic perovskites is already over 20%, suggesting them as potential future solar cell absorption materials.

The general formula of these organic−inorganic perovskites is ABX_3, where A is the organic cation ($CH_3NH_3^+$, $NH_3NH_2^+$, etc.), B can be a group IV dication such as Pb or Sn, and X can be a halogen such as Cl, Br, I. The electronic properties of these perovskites depend on their combinations, with many mixtures successfully synthesized to find improved structural stability, reproducibility, and high efficiency.[12,13] Recently, $CH_3NH_3PbI_3$ perovskite was shown experimentally to act as a photocatalyst for H_2 generation in aqueous hydrogen iodide (HI) solution.[14,15] Under visible light irradiation, $CH_3NH_3PbI_3$ powder efficiently catalyzes formation of H_2 and I_3^- in experiments. We recently reported the reaction mechanism for this photocatalysis, discovering a novel two-step Pb-activated amine-assisted (PbAAA) reaction mechanism for hydrogen evolution reaction (HER) on the $CH_3NH_3PbI_3$ surface.[16] Thus, in addition to serve as a photoabsorber for visible light, the $CH_3NH_3PbI_3$ perovskite serves as a catalyst reductant for the HER with the lead atoms and the surface organic cations both playing critical roles. We found that both H of the H_2 product are extracted from surface $CH_3NH_3^+$

Received: July 31, 2018
Published: August 4, 2018

Downloaded via SOOCHOW UNIV on March 4, 2019 at 00:43:42 (UTC).
See https://pubs.acs.org/sharingguidelines for options on how to legitimately share published articles.

ACS Publications © 2018 American Chemical Society

DOI: 10.1021/acs.jpcc.8b07380
J. Phys. Chem. C 2018, 122, 20918−20922

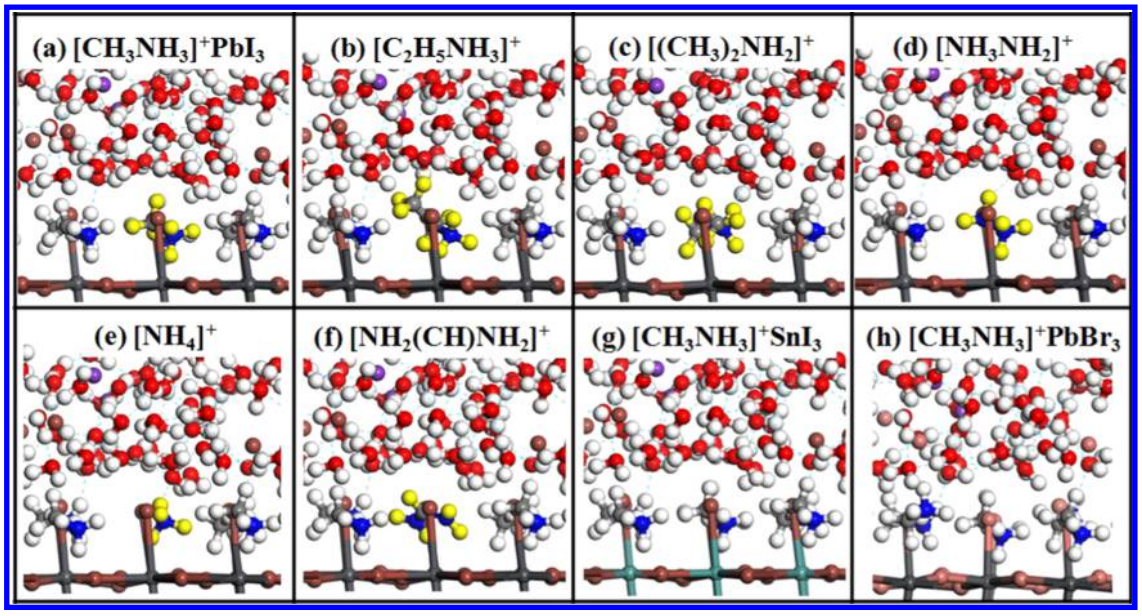

Figure 1. Optimized structures of (a) $CH_3NH_3PbI_3$ surface, with one surface $CH_3NH_3^+$ cation replaced by another organic cation, (b) $C_2H_5NH_3^+$, (c) $CH_3CH_3NH_2^+$, (d) $NH_3NH_2^+$, (e) NH_4^+, and (f) $NH_2(CH)NH_2^+$, together with the structures of (g) $CH_3NH_3SnI_3$ and (h) $CH_3NH_3PbBr_3$ in the electrode−electrolyte interface models.

cations, whereas their protons are replaced from the solution through migration along Grotthuss water chains.

Here, we report in silico studies to discover potential improved photocatalysts. To do this, we first used the two-step PbAAA reaction mechanism to examine whether the other organic cations perovskites might improve the photocatalytic efficiency. Second, we considered tin iodide perovskite as a potential lead-free photocatalyst for HER. Third, we examined Br replacement of I as the photocatalyst for H_2 production. We used the same methodology (quantum mechanics, QM) at the Perdew−Burke−Ernzerhof (PBE)-D3 level with three layers of explicit solvent to determine the reaction barriers for the photocatalytic HER reaction for five kinds of organic cations, for tin iodide perovskite, and for lead bromide perovskite.

Here, we use the 2 × 2 supercell of the (010) surface of orthorhombic $CH_3NH_3PbI_3$ as the initial structure to replace only one surface $CH_3NH_3^+$ cation by the other organic cations as a fast way to discover promising organics. For the most promising cases, we might later consider full crystals of the new organic cations or maybe a mixed system if the new organic cation prefers the surface. We derived the surfaces for lead bromide perovskite of $CH_3NH_3PbBr_3$ and the tin iodide perovskite of $CH_3NH_3SnI_3$ from their orthorhombic crystal structures. The construction of the electrode−electrolyte interface is the same as in our previous study, with 64 H_2O forming three layers over the 2 by 2 supercell.[16] To simulate the acidic environment during the HER reaction, we included three HI molecules in the solvent structure for iodide-based perovskites and three HBr molecules for bromide-based perovskites. After structural relaxation, the three HI (or HBr) molecules dissociate into three I^- (or Br^-) ions plus three H_3O^+ molecules in the solution. To describe the photoexcited state, we added two potassium atoms to populate the conduction band of the perovskite. The whole system is fully relaxed with only the bottom layer fixed.

All calculations were performed using the Vienna Ab initio Simulation Package[17,18] using the projector augmented wave method to account for core-valence interactions.[19,20] The Perdew−Burke−Ernzerhof (PBE) functional[21] of density functional theory, including the D3 van der Waals correction, was used.[22] The kinetic energy cutoff for plane wave expansions was set to 350 eV, and reciprocal space was sampled using the Γ-point scheme. We applied Gaussian smearing using a small width of 0.05 eV. Transition-state (TS) searches were conducted using the climbing image nudged elastic band method to generate the reaction path and the transition-state structure.[23] All initial state and final state geometries were converged to within 5×10^{-2} eV/Å for maximal components of forces, and the forces on TS structures were converged to 0.1 eV/Å.

We examined five different organic cations to replace one $CH_3NH_3^+$ cation on the $CH_3NH_3PbI_3$ surface: $C_2H_5NH_3^+$, $(CH_3)_2NH_2^+$, $NH_3NH_2^+$, NH_4^+, and $NH_2(CH)NH_2^+$, which are popular cations for organic−inorganic hybrid perovskites. Compared to the size of the $CH_3NH_3^+$ cation (radius of 217 pm), the effective radii of $C_2H_5NH_3^+$, $(CH_3)_2NH_2^+$, and $NH_2(CH)NH_2^+$ are larger with 274, 272, and 253 pm, respectively. The size of the $NH_3NH_2^+$ cation is the same as $CH_3NH_3^+$ (217 pm), and the effective radius of the NH_4^+ cation is the smallest with 146 pm.[24] The optimized surface structures are shown in Figure 1. After structural optimizations, the orientations of the organic cations on the surface partitioned into two groups. One group [$NH_3NH_2^+$, $(CH_3)_2NH_2^+$, and NH_4^+] leads to optimum orientations with the amine end upward to form a hydrogen bond with an H_2O in the solution, whereas the other group [$CH_3NH_3^+$, $NH_2(CH)NH_2^+$, and $C_2H_5NH_3^+$] prefers downward orientations to form a hydrogen bond with an I atom in the PbI layer. During the reactions, these groups can flip.

Taking the doped organic cation as the active site for the HER reaction, we find the same two-step PbAAA reaction mechanism for each case. Denoting the organic cations as X−H^+ and the neutral organic molecule after losing one H^+ as X, the PbAAA reaction pathway for H_2 generation in acidic HI solvent can be written as

(I) Pb activation: $X{-}H^+ + Pb + 2e^- \rightarrow X + PbH^-$,

DOI: 10.1021/acs.jpcc.8b07380
J. Phys. Chem. C 2018, 122, 20918−20922

followed by X reprotonation:

$$H_3O^+ + X \rightarrow X - H^+ + H_2O \quad (1)$$

(II) H_2 formation: $PbH^- + X{-}H^+ \rightarrow Pb + X + H_2$,

followed by X reprotonation:

$$H_3O^+ + X \rightarrow X - H^+ + H_2O \quad (2)$$

This two-step HER reaction process on the $CH_3NH_3PbI_3$ surface, doped with one $NH_2(CH)NH_2^+$ cation, is shown in Figure 2a as the representative with the initial structure,

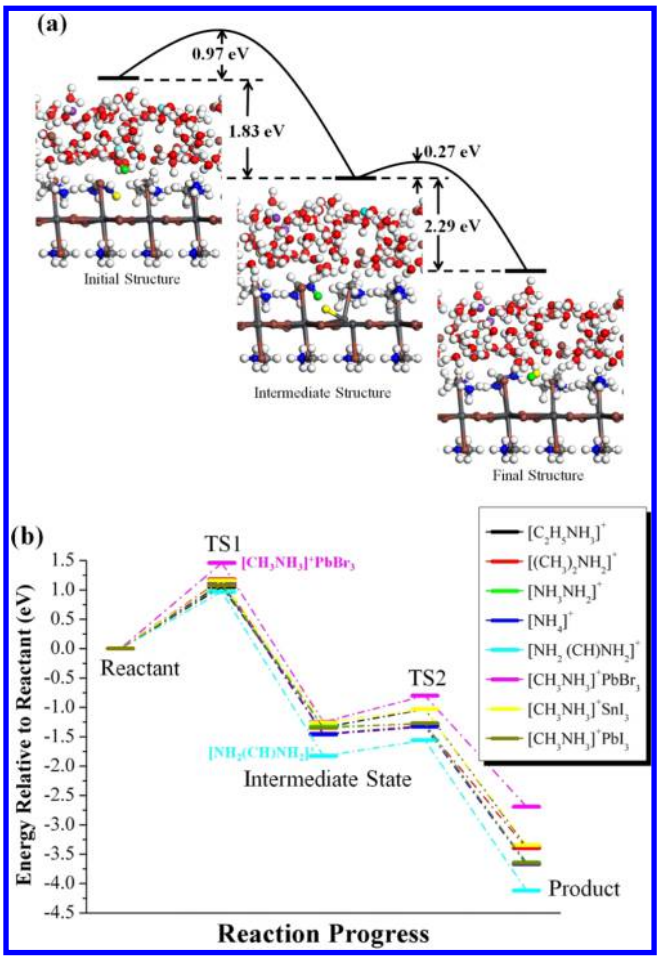

Figure 2. (a) Reaction pathway for H_2 generation at the $NH_2(CH)NH_2^+$ site on the $CH_3NH_3PbI_3$ surface in acidic solution; (b) the energetics (relative to reactant) for various organic−inorganic hybrid perovskites. The green and the yellow balls indicate two H from $NH_2(CH)NH_2^+$ to form H_2, and the cyan color indicates two protons in the solution that are involved in the Grotthuss chains.

intermediate structure, and final structure. The activation barriers and reaction energies, together with the H−Pb bond length in the intermediate structure for different organic lead iodide perovskites, are summarized in Table 1.

Pb Activation. First, the H in the $X{-}H^+$ migrates to the Pb in the PbI layer, forming PbH^- hydride intermediate. Prior to bonding to the H, the Pb had four equal Pb−I bonds (~3.2 Å) in the PbI_2 plane, each formally involving transfer of 1/2 electron from Pb to I. Formation of the Pb−H bond requires one sp hybrid on the Pb to bond to the H, leaving only one electron to share with the four I in the PbI_2 plane. The result is that, in all the cases, two of the Pb−I bonds increase their bond length to 3.7 Å, whereas the other two Pb−I bonds remain at 3.2 Å.

First Reprotonation. After the H migrates from $X{-}H^+$ cation to Pb, leaving behind a neutral X molecule, one H^+ transfers through a Grotthuss chain from the solution to the X molecule to form a new $X{-}H^+$ cation.[25] Here, by consuming one proton from the solution and two electrons, the smallest activation barrier to form the intermediate state of PbH^- hydride is found for $NH_2(CH)NH_2^+$ with 0.97 eV, which also leads to the largest reaction energy of −1.83 eV. The decreased activation barrier likely arises from the conjugation in $NH_2(CH)NH_2^+$, with delocalized electrons to facilitate the dehydrogenation of H^+ from $-NH_2^+$ to form PbH^- hydride.

Hydrogen Evolution Step. Starting from the intermediate PbH^- hydride with a Pb−H bond distance of 1.963 Å (taking $NH_2(CH)NH_2^+$ as an example), another H^+ migrates from a $NH_2(CH)NH_2^+$ to react with PbH to generate H_2, while regenerating the PbI_4 complex. This energy barrier is 0.27 eV with the reaction energy decreasing by 2.29 eV.

Second Reprotonation. A second proton from solution transfers through a Grotthuss chain to reprotonate the neutral $NH_2(CH)NH$ molecule to form a new $NH_2(CH)NH_2^+$ cation.

Thus, over the whole photocatalytic HER reaction process, the surface structure with one $NH_2(CH)NH_2^+$ cation releases a total energy of 4.12 eV by consuming two electrons and two protons. This is larger than that for the other doping cations, making $NH_2(CH)NH_2PbI_3$ as the most promising new photocatalyst for HER reaction. In Table 1, we compare the predicted barriers and energy release with the experimental gas phase proton affinities. We see that $NH_2(CH)NH_2^+$ possesses the largest proton affinity of 9.85 eV compared to the other molecules, indicating that it would have the largest energy release, which is consistent with our simulation results (energy release of 1.83 eV in the first step, larger than $CH_3NH_3^+$ with 1.35 eV). Thus, we suggest that the organic perovskite with the amine cations possessing a larger proton affinity likely exhibits a better HER performance.

Lead Free. In addition to doping of the surface cation, we also considered the lead-free tin-based perovskite. The electronegativity of Sn (2.0) is similar to Pb (2.3) while the Sn−H bond strength is larger, so we expected to a similar activation barrier for the formation of the intermediate metal hydride bond, which is the rate-determining step for the HER reaction. Using the same 2 × 2 supercell of the (010) surface of orthorhombic $CH_3NH_3SnI_3$ structure as the initial surface configuration, we find that the energy barriers for the two-step HER reaction with the lead-free $CH_3NH_3SnI_3$ surface are 1.16 and 0.23 eV, with a total reaction energy decrease of 3.35 eV, which are slightly less favorable than $CH_3NH_3PbI_3$. Extrapolating from our in silico calculations, we suggest that $NH_2(CH)NH_2SnI_3$ perovskite might be the most promising lead-free candidate, with a reaction rate comparable to $CH_3NH_3PbI_3$.

Iodine Free. We also considered the bromine-based perovskite as a candidate to replace I. We examined the same 2 × 2 supercell of the (010) surface of orthorhombic $CH_3NH_3PbBr_3$ structure as the initial surface configuration. The activation barriers for the two-step HER reaction on the $CH_3NH_3PbBr_3$ surface are calculated to be 1.46 and 0.45 eV, which are much higher than the results for $CH_3NH_3PbI_3$. To form the intermediate state of PbH^- hydride, two Pb−I (or Pb−Br) bonds in the PbI (or PbBr) layer should be broken. The bond dissociation energy for the Pb−Br bond is 2.57 eV, which is larger than the Pb−I bond of 2.01 eV, which may

DOI: 10.1021/acs.jpcc.8b07380
J. Phys. Chem. C 2018, 122, 20918−20922

Table 1. Activation Barriers (E_{a1} and E_{a2}) and Reaction Energies (E_{r1} and E_{r2}) for the Two-Step HER Reaction on Various Organic−Inorganic Perovskites Surfaces[a]

	E_{a1} (eV)	E_{r1} (eV)	H−Pb(Sn) bond length (Å)	E_{a2} (eV)	E_{r2} (eV)	PA (eV)
$[CH_3NH_3]^+PbI_3$	1.08	−1.35	1.970	0.08	−2.30	9.32
$[C_2H_5NH_3]^+$	1.05	−1.34	1.976	0.31	−2.03	9.45
$[(CH_3)_2NH_2]^+$	1.18	−1.45	1.981	0.14	−1.95	9.63
$[NH_3NH_2]^+$	1.10	−1.33	1.977	0.05	−2.31	8.84
$[NH_4]^+$	1.11	−1.46	1.968	0.13	−2.21	8.85
$[NH_2(CH)NH_2]^+$	0.97	−1.83	1.963	0.27	−2.29	9.85
$[CH_3NH_3]^+PbBr_3$	1.46	−1.25	1.987	0.45	−1.44	
$[CH_3NH_3]^+SnI_3$	1.16	−1.26	1.853	0.23	−2.09	

[a]Also shown is the experimental proton affinity (PA).[26,27] We also include H−Pb (H−Sn) bond length in the intermediate structure. We see that $[NH_2(CH)NH_2]PbI_3$ is predicted to be the best.

explain why the Br case leads to a larger barrier. The reaction energy for the whole HER reaction process decreases by 2.69 eV on the lead bromide perovskite surface, which is smaller than the results on the lead iodide perovskites, especially on the second reaction step with 1.44 eV (compared to >2.0 eV for the lead iodide perovskites). Therefore, based on our simulation results, the bromine-based perovskites are less promising than the iodine-based perovskites as photocatalysts for HER reaction to generate H_2.

The activation barriers and reaction energies for the two-step HER reaction on the different types of organic−inorganic hybrid perovskites are plotted in Figure 2b. We see clearly that $NH_2(CH)NH_2PbI_3$ (plotted in cyan color) is predicted to be the best new candidate for photocatalytic HER. Using Eyring transition-state theory, we estimate that the rate of the HER reaction on the surface $NH_2(CH)NH_2^+$ site will be improved by a factor of 10 at 300 K compared to the pristine $CH_3NH_3PbI_3$ surface.

Summarizing, we carried out QM calculations with three layers of explicit solvent for the photocatalytic HER reaction on several modifications of the $CH_3NH_3PbI_3$ perovskite surface for photochemical H_2 generation. For each case, we find the same two-step metal-activated amine-assisted reaction mechanism for HER. Comparing the various organic cations, we estimate that $NH_2(CH)NH_2^+$ cations on the surface may improve photocatalytic efficiency of the HER reaction by decreasing the barrier of 0.11 eV, which at 300 K would increase the rate by 10-fold. The bromine-based perovskites are less promising than the iodine-based perovskites as the photocatalyst for the HER reaction.

■ ASSOCIATED CONTENT

Supporting Information

The Supporting Information is available free of charge on the ACS Publications website at DOI: 10.1021/acs.jpcc.8b07380.

Geometry and energy differences (PDF)

■ AUTHOR INFORMATION

Corresponding Authors

*E-mail: wag@wag.caltech.edu (W.A.G.).
*E-mail: yyli@suda.edu.cn (Y.L.).

ORCID

Lu Wang: 0000-0001-5263-3123
William A. Goddard, III: 0000-0003-0097-5716
Tao Cheng: 0000-0003-4830-177X
Youyong Li: 0000-0002-5248-2756

Notes

The authors declare no competing financial interest.

■ ACKNOWLEDGMENTS

This work was supported by the National Key Research and Development Program of China (Grants 2018YFB0703900, 2017YFA0204800 and 2017YFB0701600), the National Natural Science Foundation of China (51761145013, 21673149). This research was also supported by the Joint Center for Artificial Photosynthesis, a DOE Energy Innovation Hub, supported through the Office of Science of the U.S. Department of Energy under Award No. DE-SC0004993. The work was carried out at National Supercomputer Center in Tianjin, and the calculations were performed on TianHe-1 (A). This project is also supported by the Fund for Collaborative Innovation Center of Suzhou Nano Science & Technology, the Priority Academic Program Development of Jiangsu Higher Education Institutions.

■ REFERENCES

(1) Schrauzer, G. N.; Guth, T. D. Photocatalytic reactions. 1. Photolysis of water and photoreduction of nitrogen on titanium dioxide. *J. Am. Chem. Soc.* **1977**, *99*, 7189.

(2) Fujishima, A.; Honda, K. Electrochemical photolysis of water at a semiconductor electrode. *Nature* **1972**, *238*, 37.

(3) Aliev, A. S.; Mamedov, M. N.; Abbasov, M. T. Photoelectrochemical properties of TiO_2/CdS heterostructures. *Inorg. Mater.* **2009**, *45*, 965.

(4) Kim, J.; Lee, C. W.; Choi, W. Platinized WO_3 as an environmental photocatalyst that generates OH radicals under visible light. *Environ. Sci. Technol.* **2010**, *44*, 6849.

(5) Sun, Y.; Sun, Z.; Gao, S.; Cheng, H.; Liu, Q.; Piao, J.; Yao, T.; Wu, C.; Hu, S.; Wei, S.; Xie, Y. Fabrication of flexible and freestanding zinc chalcogenide single layers. *Nat. Commun.* **2012**, *3*, No. 1057.

(6) Wang, X.; Maeda, K.; Thomas, A.; Takanabe, K.; Xin, G.; Carlsson, J. M.; Domen, K.; Antonietti, M. A metal-free polymeric photocatalyst for hydrogen production from water under visible light. *Nat. Mater.* **2009**, *8*, 76.

(7) Chang, K.; Mei, Z.; Wang, T.; Kang, Q.; Ouyang, S.; Ye, J. MoS_2/graphene cocatalyst for efficient photocatalytic H_2 evolution under visible light irradiation. *ACS Nano* **2014**, *8*, 7078.

(8) Burschka, J.; Pellet, N.; Moon, S.-J.; Humphry-Baker, R.; Gao, P.; Nazeeruddin, M. K.; Gratzel, M. Sequential deposition as a route to high-performance perovskite-sensitized solar cells. *Nature* **2013**, *499*, 316.

(9) Xing, G.; Mathews, N.; Sun, S.; Lim, S. S.; Lam, Y. M.; Grätzel, M.; Mhaisalkar, S.; Sum, T. C. Long-range balanced electron- and hole-transport lengths in organic-inorganic $CH_3NH_3PbI_3$. *Science* **2013**, *342*, 344.

(10) Miyata, A.; Mitioglu, A.; Plochocka, P.; Portugall, O.; Wang, J. T.-W.; Stranks, S. D.; Snaith, H. J.; Nicholas, R. J. Direct

DOI: 10.1021/acs.jpcc.8b07380
J. Phys. Chem. C 2018, 122, 20918−20922

measurement of the exciton binding energy and effective masses for charge carriers in organic−inorganic tri-halide perovskites. *Nat. Phys.* **2015**, *11*, 582.
(11) Stranks, S. D.; Eperon, G. E.; Grancini, G.; Menelaou, C.; Alcocer, M. J. P.; Leijtens, T.; Herz, L. M.; Petrozza, A.; Snaith, H. J. Electron-hole diffusion lengths exceeding 1 micrometer in an organometal trihalide perovskite absorber. *Science* **2013**, *342*, 341.
(12) Jesper Jacobsson, T.; Correa-Baena, J.-P.; Pazoki, M.; Saliba, M.; Schenk, K.; Gratzel, M.; Hagfeldt, A. Exploration of the compositional space for mixed lead halogen perovskites for high efficiency solar cells. *Energy Environ. Sci.* **2016**, *9*, 1706.
(13) Saliba, M.; Matsui, T.; Seo, J.-Y.; Domanski, K.; Correa-Baena, J.-P.; Nazeeruddin, M. K.; Zakeeruddin, S. M.; Tress, W.; Abate, A.; Hagfeldt, A.; Gratzel, M. Cesium-containing triple cation perovskite solar cells: improved stability, reproducibility and high efficiency. *Energy Environ. Sci.* **2016**, *9*, 1989.
(14) Park, S.; Chang, W. J.; Lee, C. W.; Park, S.; Ahn, H.-Y.; Nam, K. T. Photocatalytic hydrogen generation from hydriodic acid using methylammonium lead iodide in dynamic equilibrium with aqueous solution. *Nat. Energy* **2016**, *2*, No. 16185.
(15) Yaqiang, W.; Peng, W.; Xianglin, Z.; Qianqian, Z.; Zeyan, W.; Yuanyuan, L.; Guizheng, Z.; Ying, D.; Myung-Hwan, W.; Baibiao, H. Composite of $CH_3NH_3PbI_3$ with Reduced Graphene Oxide as a Highly Efficient and Stable Visible-Light Photocatalyst for Hydrogen Evolution in Aqueous HI Solution. *Adv. Mater.* **2018**, *30*, No. 1704342.
(16) Wang, L.; Xiao, H.; Cheng, T.; Li, Y.; Goddard, W. A. Pb-activated amine-assisted photocatalytic hydrogen evolution reaction on organic−inorganic perovskites. *J. Am. Chem. Soc.* **2018**, *140*, 1994.
(17) Kresse, G.; Furthmüller, J. Efficient iterative schemes for ab initio total-energy calculations using a plane-wave basis set. *Phys. Rev. B* **1996**, *54*, No. 11169.
(18) Kresse, G.; Hafner, J. Ab initio molecular dynamics for liquid metals. *Phys. Rev. B* **1993**, *47*, No. 558.
(19) Blöchl, P. E. Projector augmented-wave method. *Phys. Rev. B* **1994**, *50*, No. 17953.
(20) Kresse, G.; Joubert, D. From ultrasoft pseudopotentials to the projector augmented-wave method. *Phys. Rev. B* **1999**, *59*, No. 1758.
(21) Perdew, J. P.; Burke, K.; Ernzerhof, M. Generalized gradient approximation made simple. *Phys. Rev. Lett.* **1996**, *77*, No. 3865.
(22) Grimme, S.; Antony, J.; Ehrlich, S.; Krieg, H. A consistent and accurate ab initio parametrization of density functional dispersion correction (DFT-D) for the 94 elements H-Pu. *J. Chem. Phys.* **2010**, *132*, No. 154104.
(23) Henkelman, G.; Uberuaga, B. P.; Jónsson, H. A climbing image nudged elastic band method for finding saddle points and minimum energy paths. *J. Chem. Phys.* **2000**, *113*, 9901.
(24) Saparov, B.; Mitzi, D. B. Organic−inorganic perovskites: structural versatility for functional materials design. *Chem. Rev.* **2016**, *116*, 4558.
(25) Cheng, T.; Goddard, W. A.; An, Q.; Xiao, H.; Merinov, B.; Morozov, S. Mechanism and kinetics of the electrocatalytic reaction responsible for the high cost of hydrogen fuel cells. *Phys. Chem. Chem. Phys.* **2017**, *19*, 2666.
(26) Howard, S. T.; Platts, J. A.; Coogan, M. P. Relationships between basicity, structure, chemical shift and the charge distribution in resonance-stabilized iminoamine. *J. Chem. Soc., Perkin Trans. 2* **2002**, 899.
(27) *NIST Chemistry WebBook, NIST Standard Reference Database Number 69*; Linstrom, P., Mallard, W., Eds.; National Institute of Standards and Technology: Gaithersburg, MD, 2003. http://webbook.nist.

DOI: 10.1021/acs.jpcc.8b07380
J. Phys. Chem. C 2018, 122, 20918−20922